processes

Article

A Multifunctional, Non-Constant Current Charger Based on a Dual-Switching, Bidirectional Flyback Converter

Yu-Lin Lee [1], Chang-Hua Lin [1], Po-Hao Tsai [1], Hwa-Dong Liu [2,*] and Shiue-Der Lu [3]

[1] Department of Electrical Engineering, National Taiwan University of Science and Technology, Taipei 106, Taiwan; d10807005@mail.ntust.edu.tw (Y.-L.L.); link@mail.ntust.edu.tw (C.-H.L.); m11107201@mail.ntust.edu.tw (P.-H.T.)
[2] Undergraduate Program of Vehicle and Energy Engineering, National Taiwan Normal University, Taipei 106, Taiwan
[3] Department of Electrical Engineering, National Chin-Yi University of Technology, Taichung 411, Taiwan; sdl@ncut.edu.tw
* Correspondence: hdliu@ntnu.edu.tw; Tel.: +886-2-7749-5953

Abstract: This study implements a multifunctional charger based on a dual-switching, bidirectional flyback converter (DSBFC). The proposed charger adopts seven charging methods, including the incremental-current charging, constant-voltage (CV) charging, constant-current (CC) charging, pulse-current (PC) charging, triangular-current (TC) charging, sinusoidal-current (SC) charging, and positive/negative pulse-current (Reflex) charging methods. The charging process of a lithium-ion battery is divided into three stages: an initial term, a mid-term, and a final term. In the initial term, the incremental-current charging method is used in the initial term of charging for a soft start and to inhibit an increase in temperature. In the mid-term, five charging methods, including CC, PC, TC, SC, and Reflex-current charging, are used for charging. The CV charging method prevents overcharging the lithium-ion battery in the final term. Based on our experimental results, this study compares the four charging methods (PC, TC, SC, and Reflex-current) with the CC charging method to verify their improvement of the charging speed and increase in temperature in the mid-term. The charging speeds increased by 14.38%, 14.04%, 16.36%, and 27.27%, respectively, and the rise in temperature decreased by 37.8%, 40.5%, 48.6%, and 13.51%, respectively; all performed better than the CC charging method. Finally, users can adjust the charging method of the proposed DSBFC according to the needs of batteries so as to achieve excellent performance.

Keywords: lithium-ion battery; battery charging; non-CC charging method; dual-switching; bidirectional flyback converter

check for updates

Citation: Lee, Y.-L.; Lin, C.-H.; Tsai, P.-H.; Liu, H.-D.; Lu, S.-D. A Multifunctional, Non-Constant Current Charger Based on a Dual-Switching, Bidirectional Flyback Converter. *Processes* **2022**, *10*, 1522. https://doi.org/10.3390/pr10081522

Academic Editors: Jiaqiang E and Luigi Piga

Received: 27 May 2022
Accepted: 1 August 2022
Published: 2 August 2022

1. Introduction

Lithium-ion batteries have been widely discussed in many pieces of literature in recent years [1–3]. Compared to other rechargeable batteries, their high energy-density, high operating voltage, low self-discharge rate, and broader operating temperature make lithium-ion batteries ideal for many applications, such as electric vehicles, mobile electronic equipment, energy-storage systems, and other applications. Due to cost considerations, common lithium-ion battery chargers do not often adopt complex charging-control strategies. However, the charging method of a lithium-ion battery is critical to its lifetime, charging speed, temperature-rise effect, and other aspects.

Nowadays, numerous battery-charging-control strategies have been proposed and discussed [4–13]. Jeong et al. proposed the adaptive-input ripple (AIR) maximum power-point tracking (MPPT) technique for battery charging [4]. Liu et al. discussed an automatic voltage-compensation method based on changing the charging current for the battery charger [5]. Mao et al. introduced a reconfigurable and straightforward circuit for the wireless charging system's constant-current (CC) and constant-voltage (CV) control method [6].

Jeewandara et al. investigated the machine-learning and Kalman-filter method for battery-charger control [7]. Zhang et al. explained that the time-sharing method could reduce the current ripple in the driving- and parking-charging modes for car battery chargers [8]. Alhaider et al. presented a temperature-adjusted, multistep, CC-control, applied battery-charger system [9]. Seth et al. proposed a second-order ripple-compensation control via the pre-compensation of the reference current of the battery-charger system for electric vehicles [10]. Jeon et al. studied the best constant-power-charging control strategy based on vehicle-battery charging systems [11]. Chuang et al. demonstrated the integration of the fuzzy, CC, and CV methods to regulate the charging current applied to the battery-charging system [12]. Arshadi et al. presented the phase-shedding control strategy to enhance battery-charger performance [13].

In addition to the traditional CC−CV charging method, many references have discussed other non-constant-current charging methods [14–16]. As mentioned in references [14,15], the pulse-current (PC) and sinusoidal-current (SC) charging methods for lithium batteries have better performance in terms of charging speed and temperature increase; in addition, the triangular-current (TC) charging method [15] is also of excellent research value. In reference [16], the positive/negative pulse-current (Reflex) current charging method was introduced as a charging system for lithium-ion batteries. The Reflex charging method is also known as the positive/negative pulse charging method. Like the PC charging method, its charging-current waveform adds a reverse current of short duration to each cycle to accelerate the ions' balance inside the battery, thereby improving the charging efficiency. Most studies on this topic usually only compare the CC−CV charging method with a single one instead of with multiple non-constant-current charging methods under the same test conditions.

In terms of circuit topology, many different types of isolated power converters have been discussed in battery charging [17–26]. Avila et al. raised a multicell and multiterminal, bidirectional flyback for an electric-vehicle-battery charging system [17]. Singh et al. proposed an isolated SEPIC of a primary non-rectifier for an electric-vehicle-battery charger [18]. Moury et al. discussed a new isolated converter integrating a quasi-resonant cuk converter and flyback converter based on a solar charger [19]. Yuan et al. explained a multimode, step-up LC-resonant flyback converter designed for battery chargers [20]. Kushwaha et al. integrated isolated cuk and SEPIC converters on the primary side for an electric-vehicle-battery-charger system [21]. Gupta studied a new non-rectifier, light-electric-vehicle charger, which used an isolated Luo converter on the primary side [22]. Kushwaha et al. introduced a non-rectifier for the electric-vehicle-charging system integrating Zeta and Luo converters on the primary side [23]. Lin presented a new soft-switching, direct-current converter with a wide output-voltage range for a battery charger [24]. Wu et al. proposed a new isolated, multiwinding, coupled-inductor converter applied to the battery-charging system [25]. Lin investigated a new resonant converter with a wide output-voltage with two resonant circuits on the primary and secondary sides of the transformer, respectively, for a battery charger [26].

This study utilizes a dual-switching, bidirectional flyback converter (DSBFC) to realize seven charging methods, including incremental, CV, CC, PC, TC, SC, and Reflex-current. The incremental-current charging method is used in the initial term of charging. In the mid-term of charging, five charging methods (CC, PC, TC, SC, and Reflex-current) are used for charging, respectively, to analyze their performance for comparison. The CV charging method takes charge of the charging in the final term until the batteries are fully charged. Through the experimental results, the performance of the four charging methods (PC, TC, SC, and Reflex-current) are compared with the CC charging method, where the four charging methods perform better than the CC charging method in terms of charging speed and temperature increase in the mid-term.

This study aims to describe the difference between the five charging methods (in terms of charging speed and the temperature increase). Moreover, this study also implemented a well-known flyback converter and realized seven charging methods with the same converter. The proposed charging system can realize the incremental-current charging, constant-voltage (CV) charging, constant-current (CC) charging, pulse-current (PC) charging, triangular-current (TC) charging, sinusoidal-current (SC) charging, and positive/negative pulse-current (Reflex) charging methods with the same converter via a digital controller. Compared with other charging methods in the mid-term, the SC charging method is more appropriate. If the application of the battery module places great emphasis on charging-speed improvement, the proposed charging system will consider the Reflex-current charging method.

The remainder of this paper is organized as follows: Section 2 describes the lithium-ion battery module specifications and the charger's architecture; the designs of various charging methods and dual-closed-loop control is presented in detail in Section 3. Section 4 presents the experimental results, while Section 5 includes conclusions and suggests directions for future work.

2. Specifications of the Lithium-Ion Battery Module and the Charger's Architecture

2.1. Specifications of the Lithium-Ion Battery Module

This study considers the specifications of a small/medium-sized, electric hand tools, 3C products, etc., which require 3 18650 lithium-ion cells in a 3S1P battery module. The proposed charger is responsible for charging the battery module. The cell specifications are shown in Table 1.

Table 1. Cell specifications used in this study.

Parameter	Value
Manufacturer	Sanyo
Part number	UR18650−NSX
Rated voltage	3.6 V
Rated capacity	2500 mAh
Rated charging current	1.75 A
Upper/lower cut-off voltage	4.2 V/2.5 V
Operating temperature range	−20 °C~50 °C

2.2. Charger Architecture

The implemented charger employs the DSBFC as the main circuit and an embedded digital controller, which can realize seven charging methods with the same charger. Figure 1 shows the schematic diagram of the DSBFC. First, the DSBFC utilizes the transformer TR (magnetic coupling characteristic) to achieve the isolation between the AC input and the batteries. Second, a digital controller controls the power switch and captures the battery-module voltage and the charging current. Meanwhile, the controller calculates the PWM signal for the power switches through the captured signal, depending on the different charging methods. Finally, the isolated driver transfers the PWM signal to power switches Q_1 and Q_2. The DSBFC has been specially designed for the Reflex-current charging method, having positive/negative pulse-current waveforms. When using other charging methods (incremental current, CV, CC, SC, TC, and PC), the Q_2 can be switched off. Moreover, its body diode D_1 operates as a rectifier to transfer the energy from the AC input to the batteries in the same way as a traditional flyback converter.

Figure 2 shows the schematic diagram and the key waveforms of the DSBFC without the full-bridge rectifier. As shown in Figure 2a, the architecture includes a transformer TR, a magnetizing inductor L_m, an input filter capacitor C_{in}, a power switch on the primary side Q_1, a power switch on the secondary side Q_2, a diode on the secondary side D_1, an output capacitor C_{out}, and an equivalent resistor R_{load}. L_m stores the energy and achieves the isolated energy-transfer function with the help of the TR's magnetic coupling characteristic.

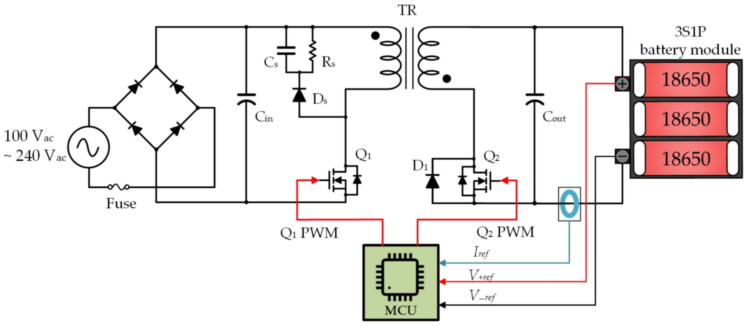

Figure 1. Schematic diagram of the DSBFC.

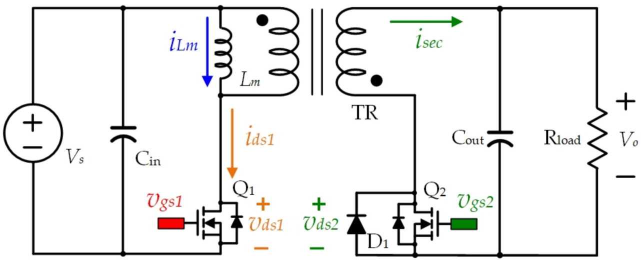

(**a**)

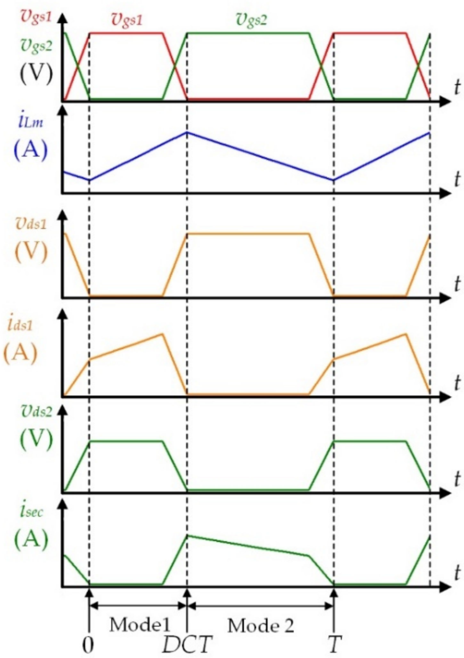

(**b**)

Figure 2. (**a**) Schematic diagram of the DSBFC without the full-bridge rectifier; (**b**) the corresponding key waveforms.

Figure 2b shows the key waveforms of the DSBFC without the full-bridge rectifier. During the steady-state operation, a period can be divided into two regions: Mode 1 is the duration when Q_1 is on; Mode 2 is the duration when Q_1 is off; *DC* is the duty cycle of Q_1, *T* is the operation period, and f_{sw} is the operating frequency.

Mode 1 (Q1 turn on):

Figure 3a shows the operation mode of Mode 1. When Q_1 turns on, Q_2 and D_1 turn off. V_s charges L_m, and L_m stores the energy. The voltage V_s is across L_m. The current i_{Lm} rises linearly, which is shown in (1). In Mode 1, the TR does not transfer the energy, and the output capacitor C_{out} discharges the energy to the R_{load}.

$$\frac{di_{Lm}}{dt} = \frac{V_s}{L_m} \tag{1}$$

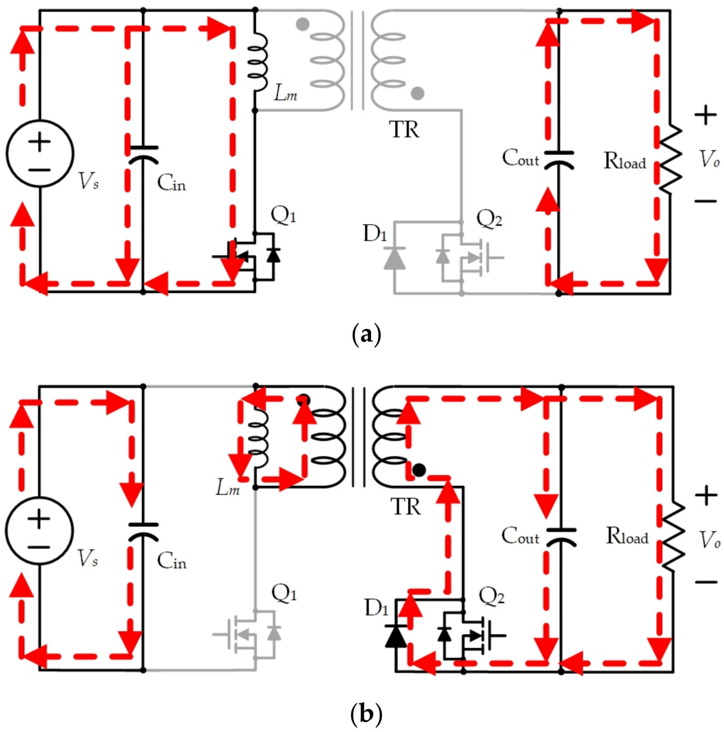

Figure 3. Operation modes of the DSBFC: (**a**) Mode 1 (Q_1 turn on), (**b**) Mode 2 (Q_1 turn off).

Mode 2 (Q_1 turn off):

Figure 3b shows the operation mode of Mode 2. When Q_1 turns off, Q_2 and D_1 turn on. Due to the characteristic of inductors, L_m projects the stored energy to the secondary side of the TR to supply the power to the output capacitor C_{out} and R_{load}. The output voltage V_o is across L_m through TR, and the current i_{Lm} decreases linearly. The formula of i_{Lm} is shown in (2), where N_1 is the turn ratio of the TR's primary side, and N_2 is the turn ratio of the TR's secondary side. In Mode 2, the TR does not transfer the energy, and the output capacitor C_{out} discharges the energy to the R_{load}.

$$\frac{di_{Lm}}{dt} = \frac{-\left(\frac{N_1}{N_2}\right)V_o}{L_m} \tag{2}$$

Integrating the Mode 1 and Mode 2 analyses, Formula (3) can be obtained by using (1) and (2), and the volt-second balance theory:

$$V_s T(DC) + \left[-\left(\frac{N_1}{N_2}\right)V_o\right](1 - DC)T = 0 \tag{3}$$

Formula (3) can be sorted out to obtain the relationship between the input voltage and the converter's output voltage, as shown in (4). From (4), it can be known that the flyback converter can achieve the purpose of boosting or bucking voltage by designing the transformer turn ratio and changing the duty cycle (DC).

$$\frac{V_o}{V_s} = \frac{DC}{1-DC}\left(\frac{N_2}{N_1}\right) \tag{4}$$

Table 2 shows the specifications and the related electrical parameters of the DSBFC, such as the transformer TR. Its input can be applied to a full AC utility power range, and its output can convert to the battery modules' upper and lower cut-off voltages.

Table 2. Specifications and related electrical parameters of the DSBFC.

Parameter	Value
Input voltage (V_s)	100 V_{ac}~240 V_{ac}
Output voltage (V_o)	7.5 V~12.6 V
Rated power (P_o)	50 W
Operating frequency (f_{sw})	100 kHz
TR's turn ratio (N_1/N_2)	146/16
TR's magnetizing inductance (L_m)	2.7 mH

Through the above analysis, it can be seen that the implemented converter can realize the energy transfer. The incremental-current charging, constant-voltage (CV) charging, constant-current (CC) charging, pulse-current (PC) charging, triangular-current (TC) charging, sinusoidal-current (SC) charging, and positive/negative pulse-current (Reflex) charging methods can be easily achieved. The chosen converter has a MOSFET paralleled with the rectifier diode D_1 so that the converter can extract the energy from the battery module back to the input capacitor C_{in}. This characteristic can help realize the Reflex charging method. However, while reversing the power flow, the voltage of the C_{in} will increase, and a dangerous situation may occur due to overcharging the C_{in}. In this study, the proposed charger is designed for small/medium-sized, electric hand tools and 3C products, which require 3 18650 lithium-ion cells in a 3S1P battery module. Moreover, the negative pulse of the implemented Reflex charging method lasts only a few microseconds, which will not cause the problem just mentioned. If the specifications of the battery module increase, the specifications of the C_{in} and additional protection should be taken into consideration.

3. Design of Various Charging Methods and Dual-Closed-Loop Control

3.1. Design of Various Charging Methods

According to the battery-module voltage, the charging strategy proposed in this paper has three stages: an initial term, a mid-term, and a final term. Figure 4 is the proposed charging strategy's schematic diagram (voltage vs. time) depending on the cell specifications. The initial term of charging is set at 7.5 V~10.2 V. During the initial term, the battery module has a significant voltage variation rate; in the mid-term, the voltage range is set at 10.2 V~12.6 V. The battery-module voltage rises gently during this stage; when the battery module reaches the upper cut-off voltage of 12.6 V, the charging strategy enters the final term (using the CV charging method).

In the initial term of charging, the incremental-current charging method, improved from the trickle method, is used to prevent the temperature from rising. The charging current increases gradually with the increase of battery-module voltage. The proposed charging strategy enters the next stage when the battery-module voltage is higher than 10.2 V. In the mid-term, the CC, SC, PC, TC, and Reflex-current charging methods are respectively implemented to control the variable for the charging-method comparison experiment. The charging strategy uses the CV charging method in the final term of charging, and the duration is decided according to the battery specifications. In this study, the final term will end when the battery reaches the upper cut-off voltage, and the charging current is less than 100 mA. The flow chart of the charging strategy is shown in Figure 5.

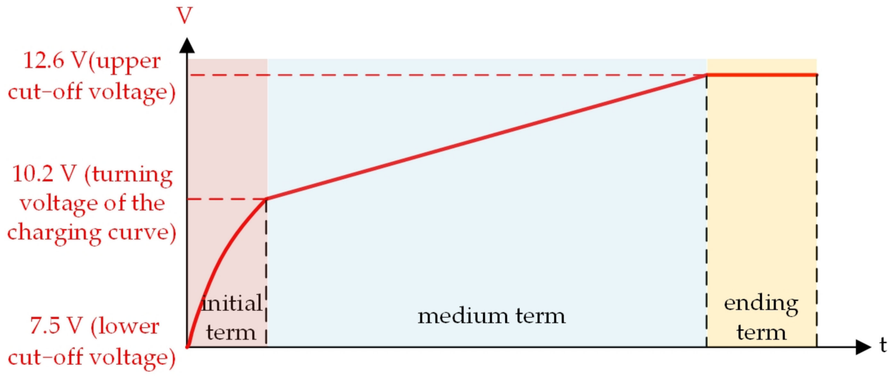

Figure 4. Schematic diagram of the proposed charging strategy.

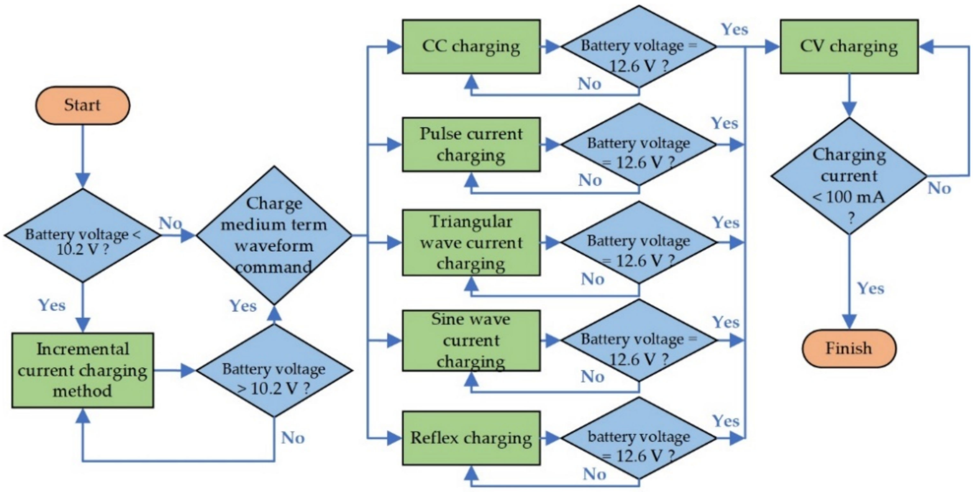

Figure 5. Flow chart of the charging strategy.

The proposed charging system uses the incremental-current charging method in the initial term and the CV charging method in the final term to control the variables. Consequently, the influence of other charging methods can be easily compared in the mid-term. In addition, according to the lithium-ion battery's characteristic, the internal impedance in the initial term is much higher than in the mid-term. In this study, the incremental-current charging method is one of the methods which can overcome the thermal issue in the initial term. Moreover, the incremental-current charging method can also provide a soft start for the proposed charging system, while the Reflex charging method (one of the charging methods to be compared) has negative pulses, probably causing the over-discharging of the battery module. Because this study aims to compare the charging methods (CC, PC, TC, SC, and Reflex-current) in a safe operation, the proposed charging system chooses the incremental-current charging method in the initial term, and the other charging methods (CC, PC, TC, SC, and Reflex-current) are applied in the mid-term.

Figure 6 shows the battery-module voltage and current waveforms in the various charging methods' initial, middle, and final stages. The incremental-current charging method is used in the initial term. Then, in the mid-term, Figure 6a shows the adoption of the CC charging method; Figure 6b shows the adoption of the PC charging method; Figure 6c shows the adoption of the TC charging method; Figure 6d shows the adoption of the SC charging method; Figure 6e shows the adoption of the Reflex-current charging method. Finally, all of the charging strategies use the CV charging method in the final term. The CC charging method will be the comparison benchmark for the other charging methods. The comparison of the charging methods evaluates their performance, such as the charging speed and charging-temperature increases in the mid-term.

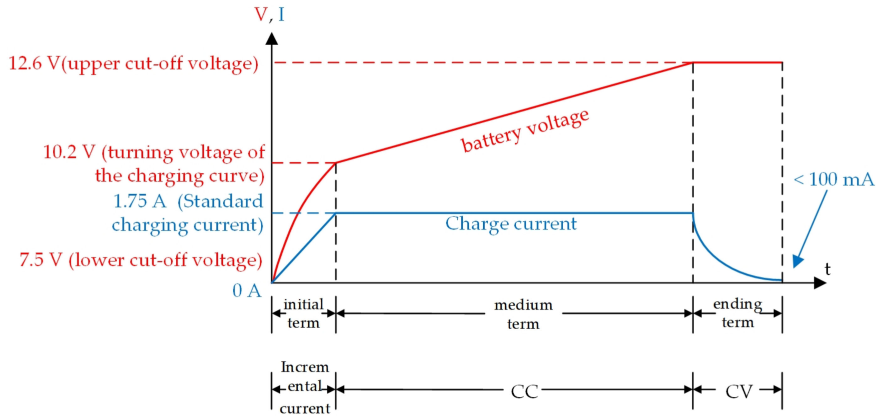

(**a**)

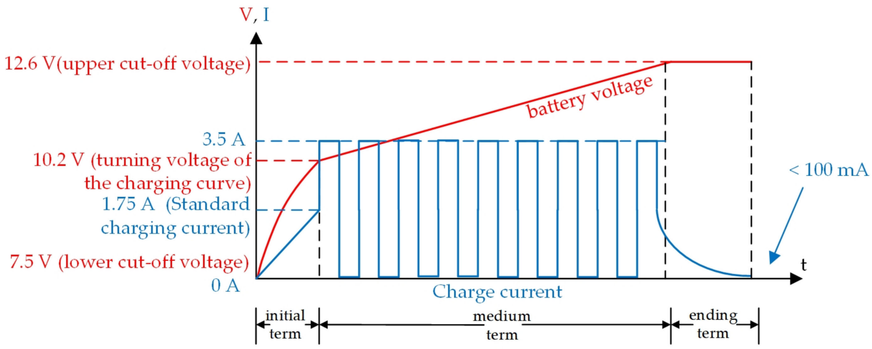

(**b**)

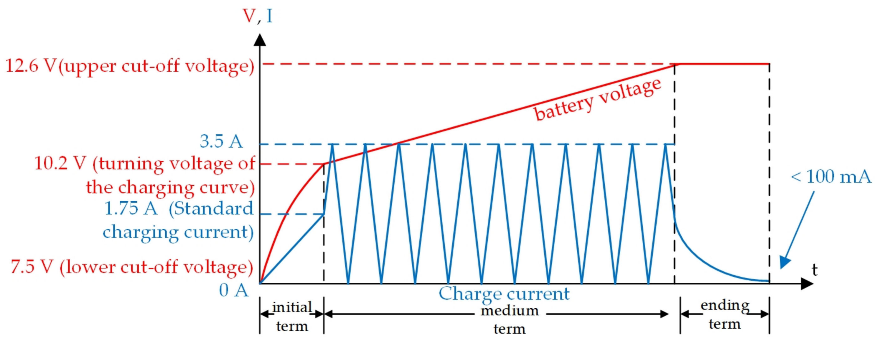

(**c**)

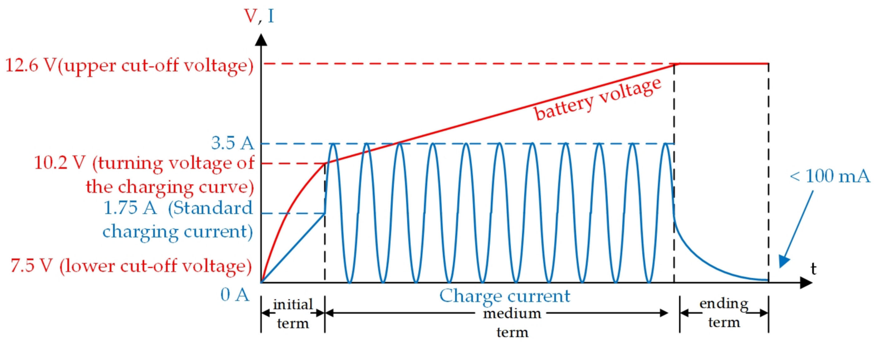

(**d**)

Figure 6. *Cont*.

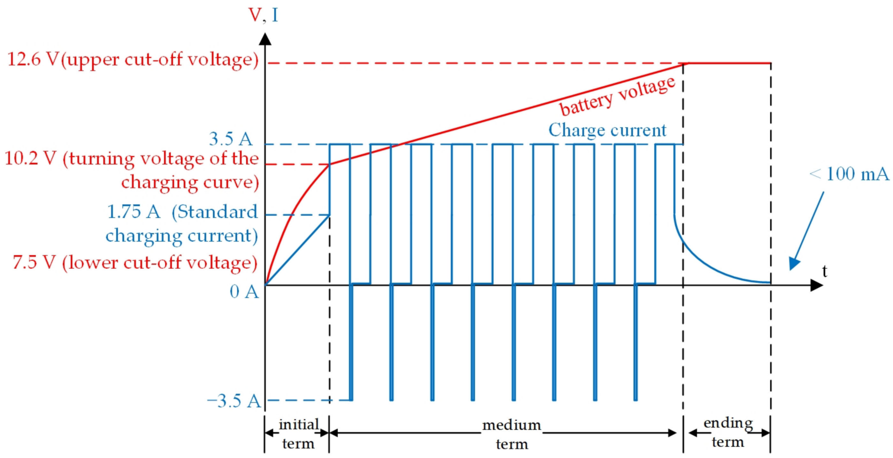

(**e**)

Figure 6. Voltage and current waveform of different charging methods used in the mid-term: (**a**) CC, (**b**) PC, (**c**) TC, (**d**) SC, and (**e**) Reflex-current.

3.2. Internal Impedance of the Lithium-Ion Cell

Figure 7 shows the frequency's influence on the lithium-ion cell's internal impedance [15]. From Figure 7, it can be seen that the minimum internal impedance of the lithium-ion cell can be obtained at the charging-current frequency f_{Zmin} of about 1 kHz, which is the crucial parameter affecting the charging speed and the temperature increase. Usually, the frequency of the non-constant current waveform is within the range of 0 Hz to 1 kHz, and the internal impedance decreases while the frequency increases. Considering the response speed of the converter hardware and digital control, the frequency setting value of the non-constant current waveform should meet the maximum when the waveform is not distorted. After the actual test, the frequency of the non-constant current waveform realized in this study was set at 4.7 Hz due to the limitations of the hardware and the prevention of the waveform distortion.

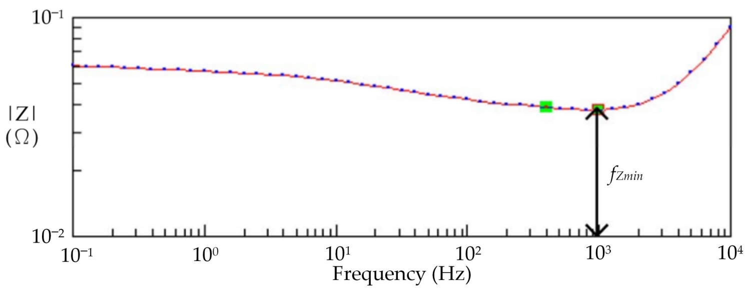

Figure 7. Relationship between the lithium-ion cell's internal impedance with charging-current frequency.

Considering the CC charging method's current value (1.75 A) as the standard charging current, the amplitude variation range of symmetrical waveforms, such as PC, TC, and SC, is 0~3.5 A. The Reflex-current charging method maintains 3.5 A for 0.6 cycle, −3.5 A for 0.1 cycle, and 0 A for the remaining 0.3 cycle. This setting ensures that the average charging current of all charging waveforms is the same and consistent. Under the same test conditions, the effects of different charging methods can be compared to show their performance.

3.3. Dual-Closed-Loop Control Design

During the charging process, the control of the converter can be divided into two parts: current closed-loop control and voltage closed-loop control. Figure 8a is the block diagram of a current closed-loop control system. The incremental-current, constant-current, and four kinds of non-constant-current charging methods are all implemented using the current-control system. The output current $\hat{i_o}$ of the converter is converted into a voltage signal by a current sensor (ACS712ELCTR−05B−T, Allegro MicroSystems, Manchester, NH, USA), sent to an analog−digital converter (ADC) with a 1023/3.3 time-rate in the digital controller (dsPIC33FJ64GS606, Microchip), and then participates in the current closed-loop control. The feedback value $i_{\hat{ADC}}$ is compared with the current command i^*_{ADC}, depending on which charging method is to be realized. This PI controller control signal of current closed-loop [$v_{\mathrm{i}}(t)$] as Equation (5), the proportional parameter K_p = 10^{-1} and the integral parameter K_i = 10^{-6}. The limiter range is 0–0.45 $\mathrm{V_{tri,pp}}$. The d^* is compared with a saw waveform signal with a frequency f^*_{sw} to generate the PWM signal S^*_1 and S^*_2 for the power switches of the converter. The corresponding switching signal is generated by the current-control system result so that the output current can achieve the current waveform to be realized. Figure 8b is the block diagram of the voltage closed-loop control system. The CV charging method is implemented using this control system, which operates similarly to the principle of the current closed-loop control system. The only difference is that the sampling signal is the output voltage. In order to ensure that the digital controller can read the output-voltage signal $\hat{v_o}$ in its limited voltage range, the output voltage $\hat{v_o}$ of the converter is bucked through a linear voltage attenuation circuit (51/200 time rate), sent to an analog−digital converter (ADC) with a 1023/3.3 time-rate in the digital controller (dsPIC33FJ64GS606, Microchip), and then participates in the voltage closed-loop control. The feedback value $v_{\hat{ADC}}$ is compared with the voltage command v^*_{ADC}, depending on which charging method is to be realized. This PI controller control signal of voltage closed-loop [$v_v(t)$] as Equation (6), K_p = 10^{-1} and K_i = 10^{-6}. The limiter range is 0–0.45 $\mathrm{V_{tri,pp}}$. The d^* is compared with a saw waveform signal with a frequency f^*_{sw} to generate the PWM signal S^*_1 and S^*_2 for the power switches of the converter.

$$v_i(t) = K_p \cdot e_i(t) + K_i \int_0^t e_i(t\prime)dt\prime \tag{5}$$

where $e_i(t)$ is $i^*_{ADC} - i_{\hat{ADC}}$ error signal.

$$v_v(t) = K_p \cdot e_v(t) + K_i \int_0^t e_v(t\prime)dt\prime \tag{6}$$

where $e_v(t)$ is $v^*_{ADC} - v_{\hat{ADC}}$ error signal.

With the help of the dual-closed-loop control system and the voltage-closed-loop control system, the incremental-current charging, constant-voltage (CV) charging, constant-current (CC) charging, pulse-current (PC) charging, triangular-current (TC) charging, sinusoidal-current (SC) charging, and positive/negative pulse-current (Reflex) charging methods can all be realized with the proposed charging system. It also has the potential to carry out other kind of charging methods.

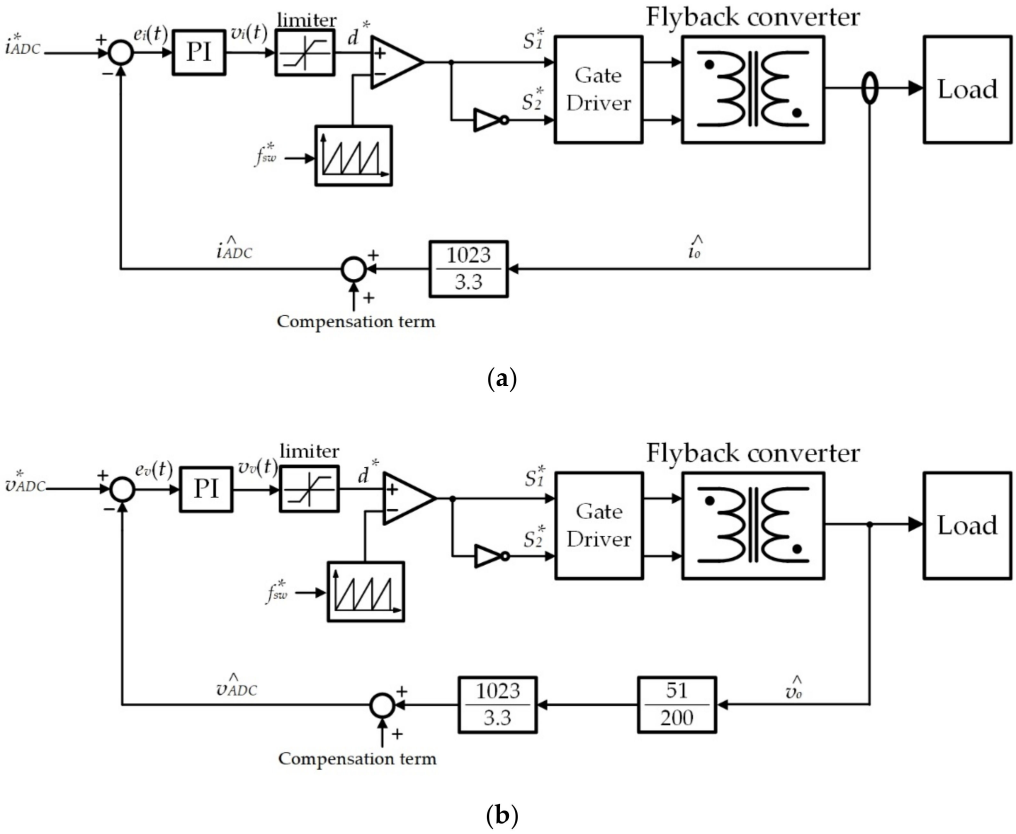

Figure 8. Diagram of the dual-closed-loop control system: (**a**) current closed-loop; (**b**) voltage closed-loop.

4. Experimental Results

Figure 9 shows the laboratory setup diagram of the battery-charging system in this study, where Figure 9a shows the overall view of the experiment, Figure 9b is a photograph of the DSBFC and the 3S1P battery module, including the actual connection. The charger implemented can use the full range of input AC power supply (100~240 V_{ac}). A digital oscilloscope records the battery-module terminal voltage and charging-current waveforms during the charging process. Meanwhile, an infrared thermometer is used for temperature monitoring. All of the charging methods have similar parameters: the frequencies are 1 Hz and 4.7 Hz, the average current is 1.75 A, the environment temperature is about 26 °C, and the environmental humidity is about 65%. The duty cycle ranges from 0~45%, which depends on the battery module's voltage and the current-charging method. Table 3 shows waveform setups of five charging methods. It is worth mentioning that the TC charging method has a 3.3 A/100 ms rising slope and a 3.3 A/100 ms decreasing slope. The experimental results were recorded using an oscilloscope (MDO3024). The AC power came directly from a plug with utility power (110 V_{ac}, 60 Hz). The load was the 3S1P lithium-ion battery module.

Table 3. Waveform setup of five charging methods.

Charging Method	Waveform Form	Frequency
Incremental-current	0~1.75 A	/
Constant-current	1.75 A	/
Pulse-current	0 A–3.5 A	1 Hz/4.7 Hz
Triangular-current	0 A~3.5 A	1 Hz/4.7 Hz
Sinusoidal-current	0 A~3.5 A	1 Hz/4.7 Hz
Reflex-current	–3.5 A~3.5 A	1 Hz/4.7 Hz
Constant-voltage	12.6 V	/

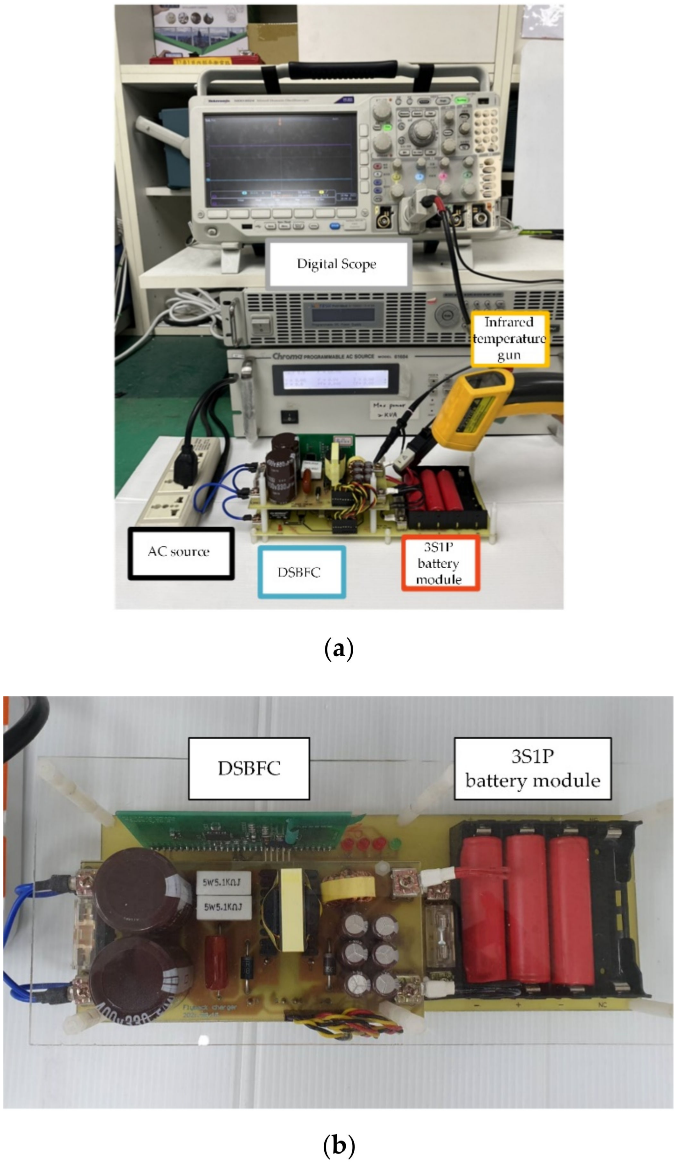

Figure 9. Laboratory setup diagram of the battery-charging system: (**a**) overall view of the experiment; (**b**) real photograph of the DSBFC and 3S1P battery module.

Figure 10 shows the V_o and I_o waveforms of the DSBFC (V_o = 12.6 V) when the output current I_o changed. The initial current of I_o was 0.75 A. The I_o suddenly increased (I_o increased to 3.5 A; indicated by the red oval), and the I_o decreased accordingly (I_o dropped to 0.75 A; indicated by the blue oval). As shown in Figure 10, the DSBFC converter can control V_o and I_o stably and rapidly, where the response time (time ≈ 10 ms) is able to realize the incremental-current charging, constant-voltage (CV) charging, constant-current (CC) charging, pulse-current (PC) charging, triangular-current (TC) charging, sinusoidal-current (SC) charging, and positive/negative pulse-current (Reflex) charging methods.

Figure 11 is a schematic diagram of a complete charging process recorded by the digital oscilloscope, and three periods can be seen according to the time axis: the initial term, the mid-term, and the final term. The mid-term of this schematic diagram takes Reflex-current charging methods as an example, and the incremental-current charging method and the constant-voltage charging method are respectively used in the initial and final terms.

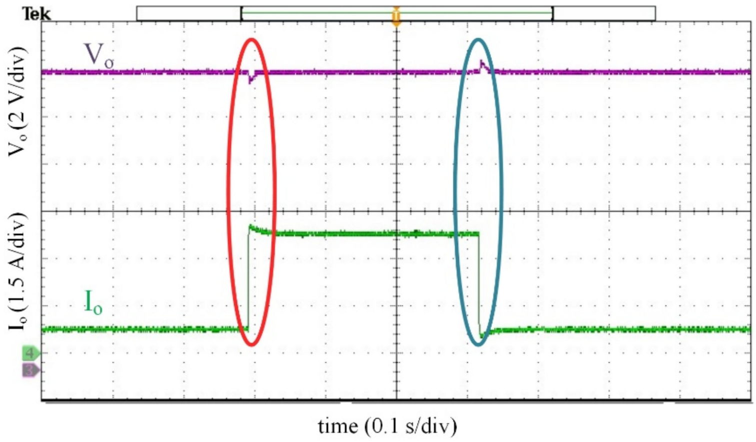

Figure 10. V_o and I_o waveforms of the DSBFC (V_o = 12.6 V) when the output current changes. (V_o: 2 V/div; I_o: 1.5 A/div; and Hor: 0.1 s/div.)

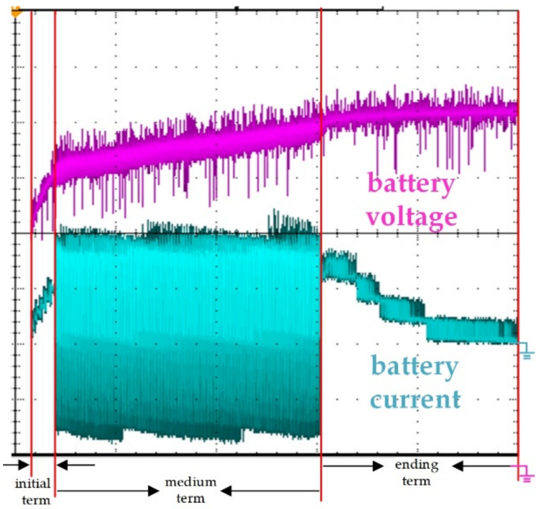

Figure 11. Battery-module voltage and charging-current waveforms during the charging process (Reflex-current charging method used in the mid-term.)

Figure 12 shows the temperature-increase curves of five charging methods. The five charging methods are the constant-current (CC), pulse-current (PC), triangular-current (TC), sinusoidal-current, and positive/negative pulse-current (Reflex-current) charging methods. The effects of these five charging methods on the charging time and the increase in temperature are recorded and then consolidated in Table 4 and in Figures 13 and 14. The CC charging method is the comparison benchmark for the other charging methods (PC, TC, SC, and Reflex-current) to verify the difference in the charging duration and temperature increase between different charging methods during the charging process.

Table 4. Experiment results of five charging methods.

Mid-Term	**Duration**		**Temperature Increase**	
	1 Hz	**4.7 Hz**	**1 Hz**	**4.7 Hz**
Constant-current	3635 s	3630 s	7.6 °C	7.4 °C
Pulse-current	3110 s	3108 s	4.7 °C	4.6 °C
Triangular-current	3130 s	3120 s	4.6 °C	4.4 °C
Sinusoidal-current	3040 s	3036 s	3.9 °C	3.8 °C
Reflex-current	2646 s	2640 s	6.7 °C	6.4 °C

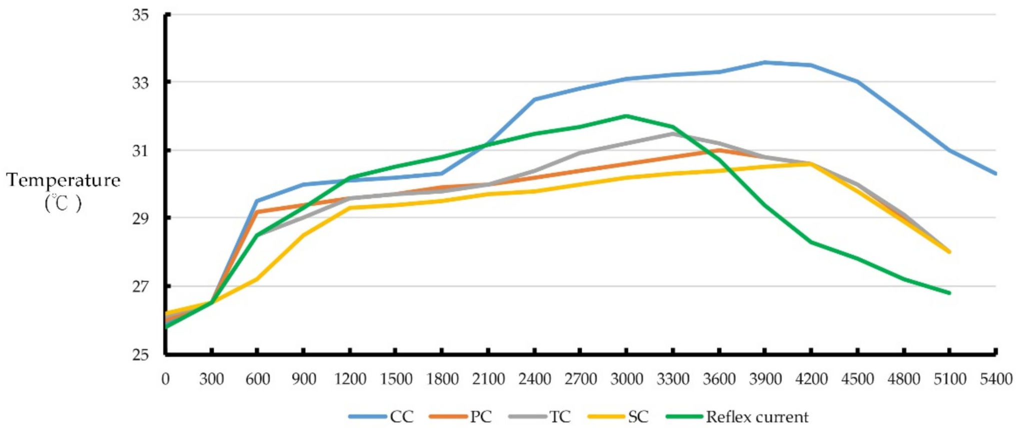

Figure 12. Temperature-increase curves of five charging methods.

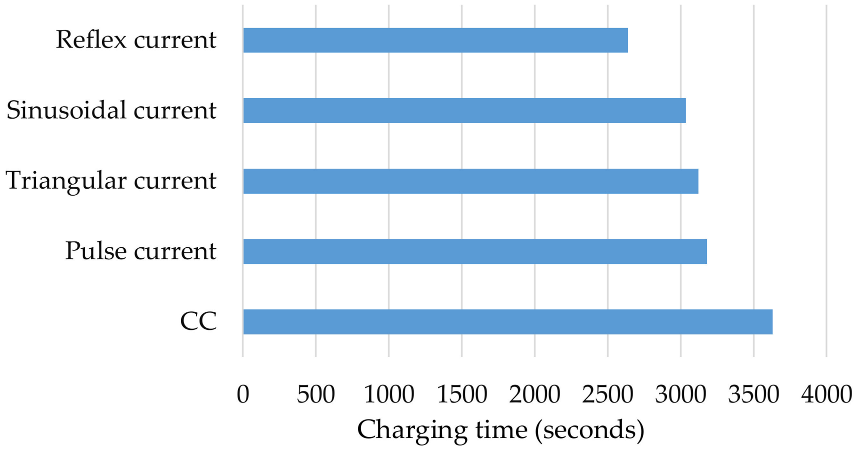

Figure 13. Charging duration comparison between five charging methods.

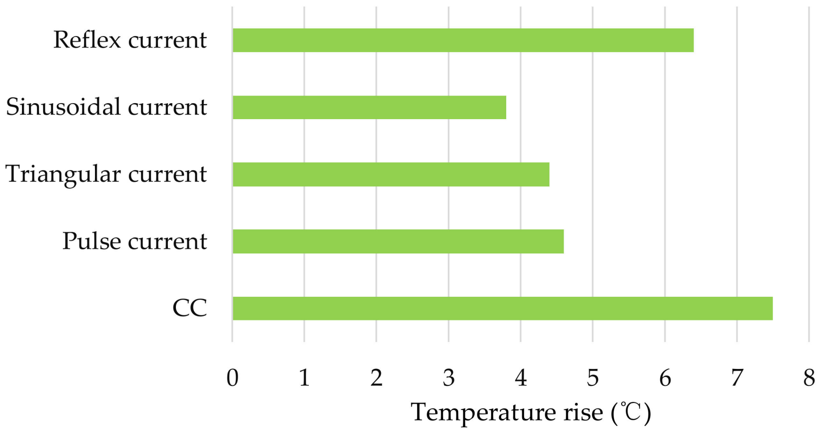

Figure 14. Charging-temperature increase comparison between five charging methods.

According to Table 4, in order to objectively compare the improvement (charging speed and temperature increase) of various non-constant-current charging methods, the following defines the improvement of charging speed (IOCS) and the improvement of temperature increase (IOTI), which both set the CC charging methods as the comparison benchmark for the other charging methods (PC, TC, SC, Reflex-current). The formulas of IOCS and IOTI are shown in (7) and (8), respectively, where t_{cc} is the charging duration using the CC charging method, and t_x is the charging duration of the other non-constant-current charging methods to be compared, T_{cc} is the temperature increase using the CC charging method, and T_x is the temperature increase of the other non-constant-current charging methods to be compared. The calculation principles of IOCS and IOTI are similar. The denominator is the experimental data of the CC charging method, and the numerator is the difference between the experimental data of the other charging method to be compared and the CC charging method.

$$\text{IOCS}(\%) = \frac{t_{cc} - t_x}{t_{cc}} \times 100 \tag{7}$$

$$\text{IOTI}(\%) = \frac{T_{cc} - T_x}{T_{cc}} \times 100 \tag{8}$$

Table 5 shows the improvement in charging speed and temperature increase of the non-constant-current charging methods under the waveform frequency = 4.7 Hz. From Table 5, it can be obtained that the waveform frequency does not affect the charging speed while having influence on the temperature increase due to the internal impedance. What is more, among these four non-constant-current charging methods, the Reflex-current charging method has the fastest charging speed, which is 27.27% faster than that of the CC charging method ($\text{IOCS}_{\text{Reflex}}$ = 27.27%); on the contrary, the Reflex-current charging method has the highest temperature-increase performance among the four charging methods. It only improves by a 13.51% temperature increase less than the CC charging method ($\text{IOTI}_{\text{Reflex}}$ = 13.51%). By contrast, the SC charging method ranks second in charging speed, which is slower than the Reflex-current charging method; however, the temperature-increase performance is the best among the four charging methods, with a 48.6% improvement ($\text{IOTI}_{\text{sinusoidal}}$ = 48.6%), which almost reduces the temperature increase by half as compared with the CC charging method.

Table 5. Improvement of the four non-constant-current charging methods compared with the CC charging method under the waveform frequency = 4.7 Hz.

Mid-Term	Charging-Speed Improvement	Temperature-Increase Improvement
Pulse-current	14.38%	37.8%
Triangular-current	14.04%	40.5%
Sinusoidal-current	16.36%	48.6%
Reflex-current	27.27%	13.51%

The proposed charging system can realize the incremental-current charging, constant-voltage (CV) charging, constant-current (CC) charging, pulse-current (PC) charging, triangular-current (TC) charging, sinusoidal-current (SC) charging, and positive/negative pulse-current (Reflex) charging methods with the same converter via the digital controller. Compared with other charging methods in the mid-term, the SC charging method was more appropriate. If the application of the battery module places great emphasis on the improvement of the charging speed, the proposed charging system will consider the Reflex-current charging method.

5. Conclusions

This study implements a multifunctional charger based on the DSBFC topology with a dual-closed-loop, which realizes seven charging methods: the incremental-current, CC, PC, TC, SC, Reflex-current, and CV charging methods. The incremental-current and constant-voltage charging methods are used in the initial and final terms of charging, respectively. In the mid-term, the CC, PC, TC, SC, and Reflex-current charging methods are respectively adopted, and the charging speeds and the temperature increases of the different charging methods are compared under the same test conditions. In the mid-term, the PC, TC, SC, and Reflex-current charging methods all perform better than the CC charging method, where the IOSCs are 14.38%, 14.04%, 16.36%, and 27.27%, respectively; their IOTIs are 37.8%, 40.5%, 48.6%, and 13.51%, respectively. The proposed multifunctional battery charger can be used in various charging methods, and the charging method can be adjusted to have excellent performance according to the user's needs and the battery-module specifications.

Two conclusions can be obtained from the measured results: First, the Reflex-current charging method can be chosen to charge batteries if there is a need for fast charging, and the battery life and heat dissipation issues are not to be considered. The experimental results in this study show that its charging speed is 27.27% faster than constant-current charging ($IOCS_{Reflex}$ = 27.27%); second, in order to improve the charging speed while considering the issue of battery heat-generation, the SC charging method would be a better choice. The experimental results show that its charging speed is 16.36% faster than the CC charging method ($IOCS_{sinusoidal}$ = 16.36%), while its temperature increase is improved by 48.6% over the CC charging method ($IOTI_{sinusoidal}$ = 48.6%).

In future work, the charger realized in this study can be simplified to reduce volume and cost in pursuit of high-performance and low hardware costs for general-purpose charger products. Furthermore, follow-up research can increase the rated power of the charger due to the higher specifications of the battery modules and add a power-factor corrector (PFC) function to the AC input to meet the application field of higher capacity batteries.

Author Contributions: Y.-L.L. and C.-H.L. conceived of the presented idea and designed the experiment; Y.-L.L. and P.-H.T. performed testing and verification; Y.-L.L., H.-D.L. and S.-D.L. wrote this article; C.-H.L. supervised the findings of this work; all authors provided critical feedback and helped shape the research, analysis, and manuscript. All authors have read and agreed to the published version of the manuscript.

Funding: This research was funded by the National Science and Technology Council, Taiwan, R.O.C., grant number MOST 110-2221-E-011-081, MOST 110-3116-F-011-002, and MOST 110-2622-8-005-005-TE1. The authors also sincerely appreciate the partial financial support from the Taiwan Building Technology Center from The Featured Areas Research Center Program within the framework of the Higher Education Sprout Project by the Ministry of Education in Taiwan.

Institutional Review Board Statement: Not applicable.

Informed Consent Statement: Not applicable.

Data Availability Statement: Not applicable.

Conflicts of Interest: The authors declare no conflict of interest.

References

1. Chang, C.-J. Study of Ni-MH Battery Capacity Management. Master's Thesis, Department of Electrical Engineering, National Sun Yat-sen University, Kaohsiung, Taiwan, 2005; pp. 1–109.
2. Liu, W.; Sun, X.; Wu, H.; He, Z.; Yang, G. A multistage current charging method for Li-ion battery bank considering balance of internal consumption and charging speed. In Proceedings of the 2016 IEEE 8th International Power Electronics and Motion Control Conference (IPEMC-ECCE Asia), Hefei, China, 22–26 May 2016; pp. 1401–1406. [CrossRef]
3. Gaglani, M.; Rai, R.; Das, S. Implementation Of Multilevel Battery Charging Scheme For Lithium-ion Batteries. In Proceedings of the 2019 National Power Electronics Conference (NPEC), Tiruchirappalli, India, 13–15 December 2019; 1–6. [CrossRef]
4. Jeong, J.; Shim, M.; Maeng, J.; Park, I.; Kim, C. A High-Efficiency Charger With Adaptive Input Ripple MPPT for Low-Power Thermoelectric Energy Harvesting Achieving 21% Efficiency Improvement. *IEEE Trans. Power Electron.* **2020**, *35*, 347–358. [CrossRef]
5. Liu, P.J.; Chen, T.F.; Yang, H.S. A Li-Ion Battery Charger With Variable Charging Current and Automatic Voltage-Compensation Controls for Parallel Charging. *IEEE J. Emerg. Sel. Top. Power Electron.* **2022**, *10*, 997–1006. [CrossRef]
6. Mao, X.; Chen, J.; Zhang, Y.; Dong, J. A Simple and Reconfigurable Wireless Power Transfer System With Constant Voltage and Constant Current Charging. *IEEE Trans. Power Electron.* **2022**, *37*, 4921–4925. [CrossRef]
7. Jeewandara, J.; Karunadasa, J.; Hemapala, K. Comprehensive Study of Kalman Filter Based State of Charge Estimation Method for Battery Energy Management System in Microgrid. In Proceedings of the 2021 International Conference on Electrical, Computer, Communications and Mechatronics Engineering (ICECCME), Mauritius, Mauritius, 7–8 October 2021; pp. 1–6. [CrossRef]
8. Zhang, Y.; Fang, J.; Gao, F.; Gao, S.; Rogers, D.J.; Zhu, X. Integrated High- and Low-Frequency Current Ripple Suppressions in a Single-Phase Onboard Charger for EVs. *IEEE Trans. Power Electron.* **2021**, *36*, 1717–1729. [CrossRef]

9. Alhaider, M.M.; Ahmed, E.M.; Aly, M.; Serhan, H.A.; Mohamed, E.A.; Ali, Z.M. New Temperature-Compensated Multi-Step Constant-Current Charging Method for Reliable Operation of Battery Energy Storage Systems. *IEEE Access* **2020**, *8*, 27961–27972. [CrossRef]
10. Seth, A.K.; Singh, M. Second-Order Ripple Minimization in Single-Phase Single-Stage Onboard PEV Charger. *IEEE Trans. Transp. Electrif.* **2021**, *7*, 1186–1195. [CrossRef]
11. Jeon, S.U.; Park, J.-W.; Kang, B.-K.; Lee, H.-J. Study on Battery Charging Strategy of Electric Vehicles Considering Battery Capacity. *IEEE Access* **2021**, *9*, 89757–89767. [CrossRef]
12. Chuang, C.-C.; Yao, C.-J.; Wu, S.-T. Study on Fast Charging Method of Series Connected Lithium-Ion Battery Strings with Intelligent Control. In Proceedings of the 2020 International Conference on Fuzzy Theory and Its Applications (iFUZZY), Hsinchu, Taiwan, 4–7 November 2020; pp. 1–6. [CrossRef]
13. Arshadi, S.A.; Ordonez, M.; Eberle, W.; Craciun, M.; Botting, C. Three-Phase LLC Battery Charger: Wide Regulation and Improved Light-Load Operation. *IEEE Trans. Power Electron.* **2021**, *36*, 1519–1531. [CrossRef]
14. Chen, L.-R.; Chen, J.-J.; Ho, C.-M.; Wu, S.-L.; Shieh, D.-T. Improvement of Li-ion Battery Discharging Performance by Pulse and Sinusoidal Current Strategies. *IEEE Trans. Ind. Electron.* **2013**, *60*, 5620–5628. [CrossRef]
15. Chen, L.-R.; Wu, S.-L.; Shieh, D.-T.; Chen, T.-R. Sinusoidal-Ripple-Current Charging Strategy and Optimal Charging Frequency Study for Li-Ion Batteries. *IEEE Trans. Ind. Electron.* **2013**, *60*, 88–97. [CrossRef]
16. Chan, S.Y.; Chang, Y.N.; Yang, Y.S.; Cheng, H.L. A Single-Stage High Power-Factor Lithium Battery Charger Having Reflex Charging Mechanism. In Proceedings of the 2017 IEEE 3rd International Future Energy Electronics Conference and ECCE Asia (IFEEC 2017–ECCE Asia), Kaohsiung, Taiwan, 3–7 June 2017; pp. 1926–1931.
17. Avila, A.; Garcia-Bediaga, A.; Alzuguren, I.; Vasić, M.; Rujas, A. Modular Multifunction Power Converter Based on a Multi-winding Flyback Transformer for EV Application. *IEEE Trans. Transp. Electrif.* **2022**, *8*, 168–179. [CrossRef]
18. Singh, B.; Kushwaha, R. A PFC Based EV Battery Charger Using a Bridgeless Isolated SEPIC Converter. *IEEE Trans. Ind. Appl.* **2020**, *56*, 477–487. [CrossRef]
19. Moury, S.; Lam, J. A Soft-Switched Power Module With Integrated Battery Interface for Photovoltaic-Battery Power Architecture. *IEEE J. Emerg. Sel.Top. Power Electron.* **2020**, *8*, 3090–3110. [CrossRef]
20. Yuan, Y.; Lai, L.; Wu, Q.; Yi, C. An Integrated Boost-LC-Resonant-Flyback Multimode Converter for Battery Charger Appli-cations. *IEEE Trans. Industr. Electron.* **2021**, *68*, 12196–12205. [CrossRef]
21. Kushwaha, R.; Singh, B.; Khadkikar, V. An Isolated Bridgeless Cuk–SEPIC Converter-Fed Electric Vehicle Charger. *IEEE Trans. Ind. Appl.* **2022**, *58*, 2512–2526. [CrossRef]
22. Gupta, J.; Singh, B. Bridgeless Isolated Positive Output Luo Converter Based High Power Factor Single Stage Charging Solution for Light Electric Vehicles. *IEEE Trans. Ind. Appl.* **2022**, *58*, 732–741. [CrossRef]
23. Kushwaha, R.; Singh, B. Bridgeless Isolated Zeta–Luo Converter-Based EV Charger With PF Preregulation. *IEEE Trans. Ind. Appl.* **2021**, *57*, 628–636. [CrossRef]
24. Lin, B.-R. Analysis and Implementation of a Bidirectional Converter with Soft Switching Operation. *Processes* **2022**, *10*, 561. [CrossRef]
25. Wu, Y.-E.; Lin, P.-J. Design of a High Efficiency High Step-Up/Step-Down Bidirectional Isolated DC–DC Converter. *Processes* **2022**, *10*, 50. [CrossRef]
26. Lin, B.-R. Bidirectional Resonant Converter for DC Microgrid Applications. *Processes* **2021**, *9*, 1664. [CrossRef]